Simulation of Energetic Neutral atoms at Mars and a Comparison with ASPERA-3 data

H. Gunell,* K. Brinkfeldt, S. Barabash, M. Holmström,† A. Ekenbäck,
Y. Futaana, R. Lundin, H. Andersson, M. Yamauchi, and A. Grigoriev
Swedish Institute of Space Physics, Kiruna, Sweden

E. Kallio, T. Säles, P. Riihela, and W. Schmidt
Finnish Meteorological Institute, Box 503 FIN-00101 Helsinki, Finland

P. Brandt, E. Roelof, D. Williams, and S. Livi
Applied Physics Laboratory, Johns Hopkins University, Laurel, MD 20723-6099, USA

J. D. Winningham, R. A. Frahm, J. R. Sharber, and J. Scherrer
Southwest Research Institute, San Antonio, TX 7228-0510, USA

A. J. Coates, D. R. Linder, and D. O. Kataria
Mullard Space Science Laboratory, University College London, Surrey RH5 6NT, UK

Hannu E. J. Koskinen
University of Helsinki, Department of Physical Sciences P.O. Box 64, 00014 Helsinki

J. Kozyra
Space Physics Research Laboratory, University of Michigan, Ann Arbor, MI 48109-2143, USA

J. Luhmann
Space Science Laboratory, University of California at Berkeley, Berkeley, CA 94720-7450, USA

C. C. Curtis, K. C. Hsieh, and B. R. Sandel
University of Arizona, Tucson, AZ 85721, USA

M. Grande and M. Carter
Rutherford Appleton Laboratory, Chilton, Didcot, Oxfordshire OX11 0QX, UK

J.-A. Sauvaud, A. Fedorov, and J.-J. Thocaven
Centre d'Etude Spatiale des Rayonnements, BP-4346, F-31028 Toulouse, France

S. McKenna-Lawlor
Space Technology Ireland., National University of Ireland, Maynooth, Co. Kildare, Ireland

S. Orsini, R. Cerulli-Irelli, and M. Maggi
Instituto di Fisica dello Spazio Interplanetari, I-00133 Rome, Italy

P. Wurz and P. Bochsler
University of Bern, Physikalisches Institut, CH-3012 Bern, Switzerland

N. Krupp, J. Woch, and M. Fränz
Max-Planck-Institut fur Aeronomie, D-37191 Katlenburg-Lindau, Germany

K. Asamura
Institute of Space and Astronautical Science, 3-1-1 Yoshinodai, Sagamichara, Japan

C. Dierker
Technical University of Braunschweig, Hans-Sommer-Strasse 66, D-38106 Braunschweig, Germany

Abstract:
We present observations of energetic neutral atoms (ENA) generated in the magnetosheath at Mars. The measurements were made with the Neutral Particle Imager (NPI) of the ASPERA-3 instrument on ESA's Mars Express mission [1]. These ENAs are the result of charge exchange collisions between solar wind protons and neutral oxygen and hydrogen in the exosphere of Mars. We compare the measured data with simulations of ENAs that are based on a analytical model of the plasma flow around Mars [2]. This model has been used to study the role of charge exchange in Mars-solar wind interaction [3], and was used by *Holmström et al.* [4] to simulate ENA images. The measurements agree with the model, and it is possible to find parameter values in the model so that many features of the observations are reproduced.

Orbit and Instrument

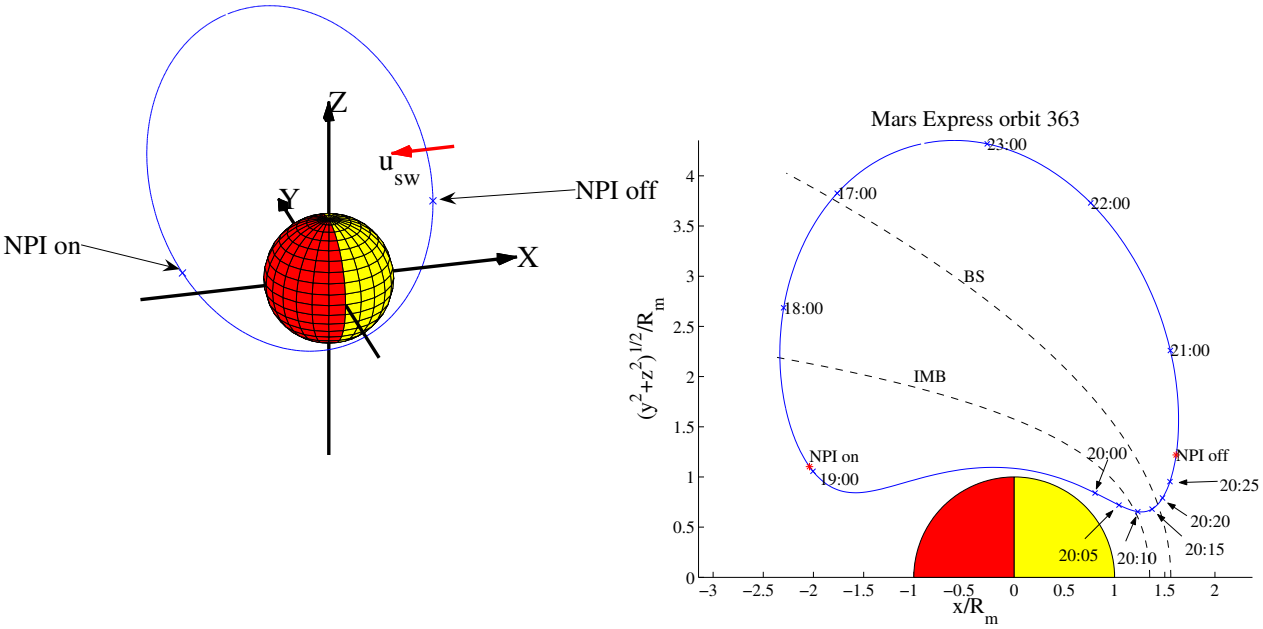

FIG. 1 Left: The coordinate system. Right: Mars Express orbit 363 in cylindrical coordinates, with the bow shock (BS) and the induced magnetosphere boundary (IMB) shown. $(y^2 + z^2)^{1/2}$ is the distance to the Mars-Sun line.

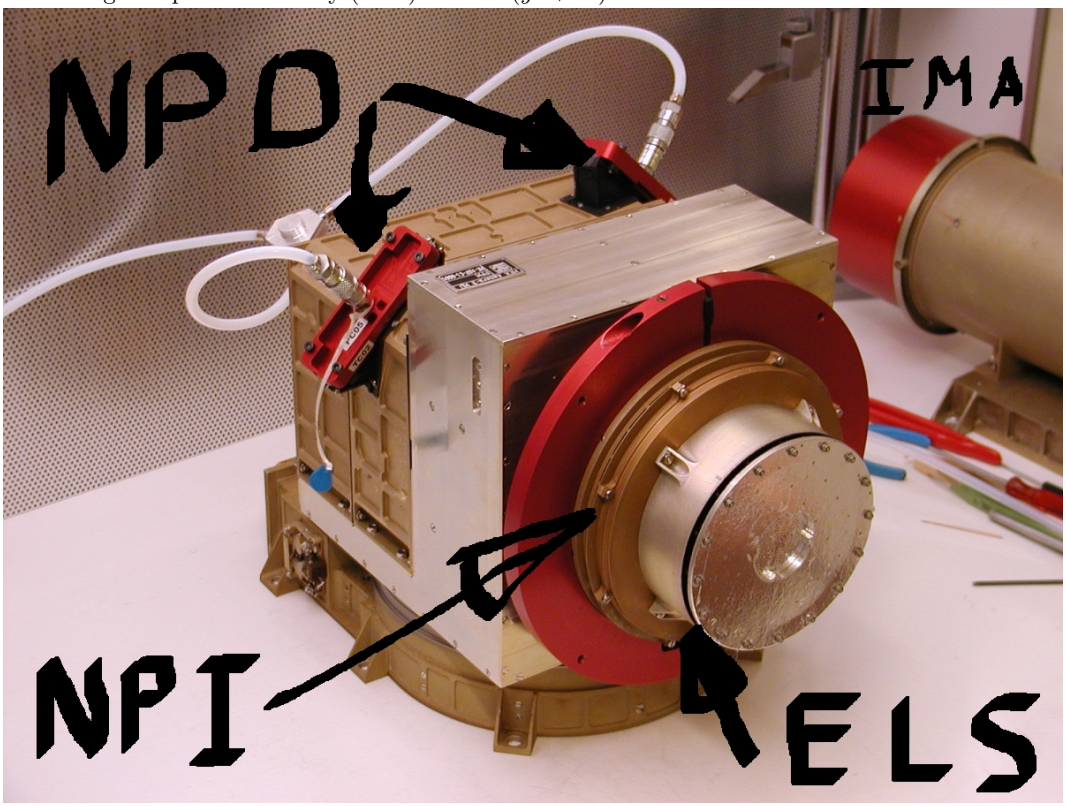

FIG. 2 The ASPERA-3 instrument.

Parameter	**NPI**	**NPD**	**ELS**	**IMA**
Particles to be measured	ENA	ENA	electrons	ions
Energy, keV per charge	≈0.1-60	0.1-10	0.01-20	0.01-40
Energy resolution, $\Delta E/E$	-	0.8	0.07	0.07
Mass resolution	-	H, O	-	m/q=1,2,4,8,16,>20
Intrinsic field of view	$9 \times 344°$	$9 \times 180°$	$10 \times 360°$	$90 \times 360°$
Angular resolution, FWHM	$4.6 \times 11.5°$	$5 \times 30°$	$10 \times 22.5°$	$4.5 \times 22.5°$
G-factor / pixel, cm^2 sr	$2.7 \cdot 10^{-3}$	$6.2 \cdot 10^{-3}$	$7 \cdot 10^{-5}$	$3.5 \cdot 10^{-4}$
Efficiency, %	≈ 1	0.1-20	incl. in G-factor	incl. in G-factor
Time resolution (full 3D), s	32	32	32	32
Mass, kg	0.7	1.3	0.3	2.2
Power, W	0.8	1.5	0.6	3.5

Observations

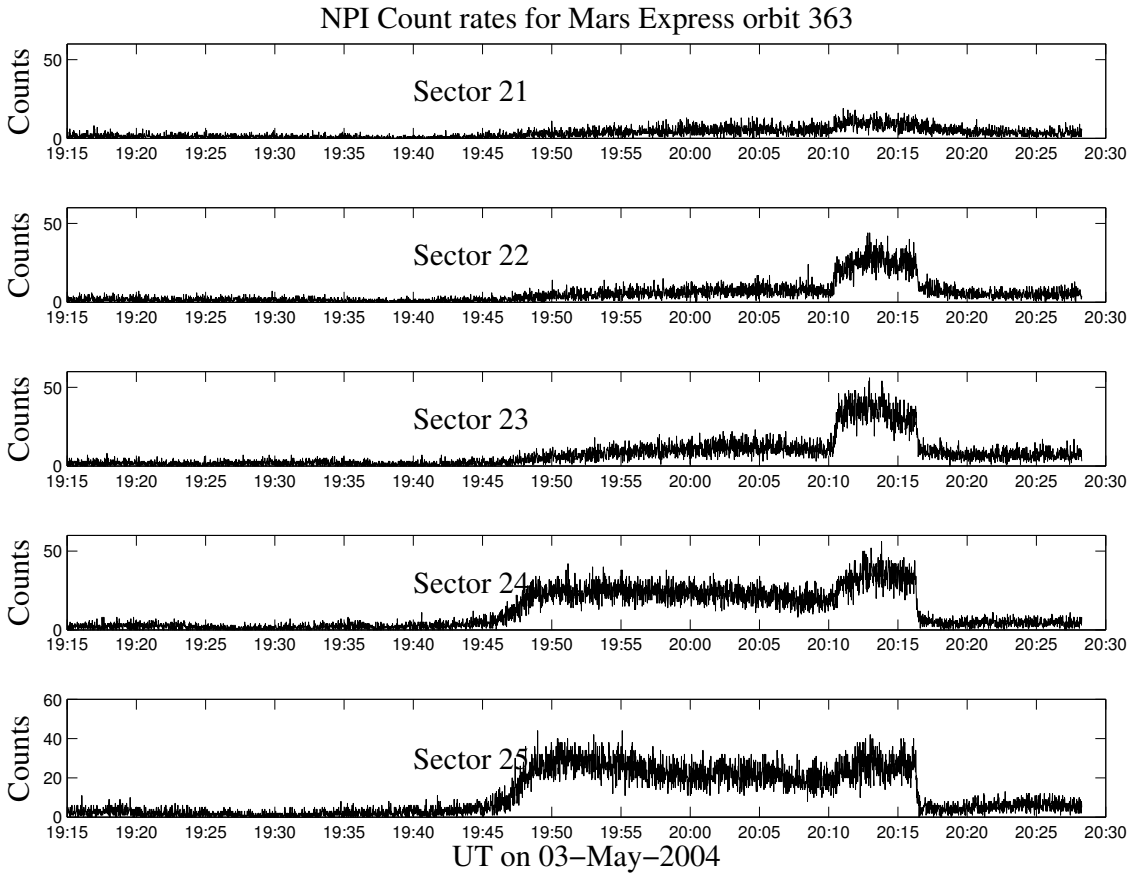

FIG. 3 Orbit 363 data from the ASPERA-3 NPI sensor.

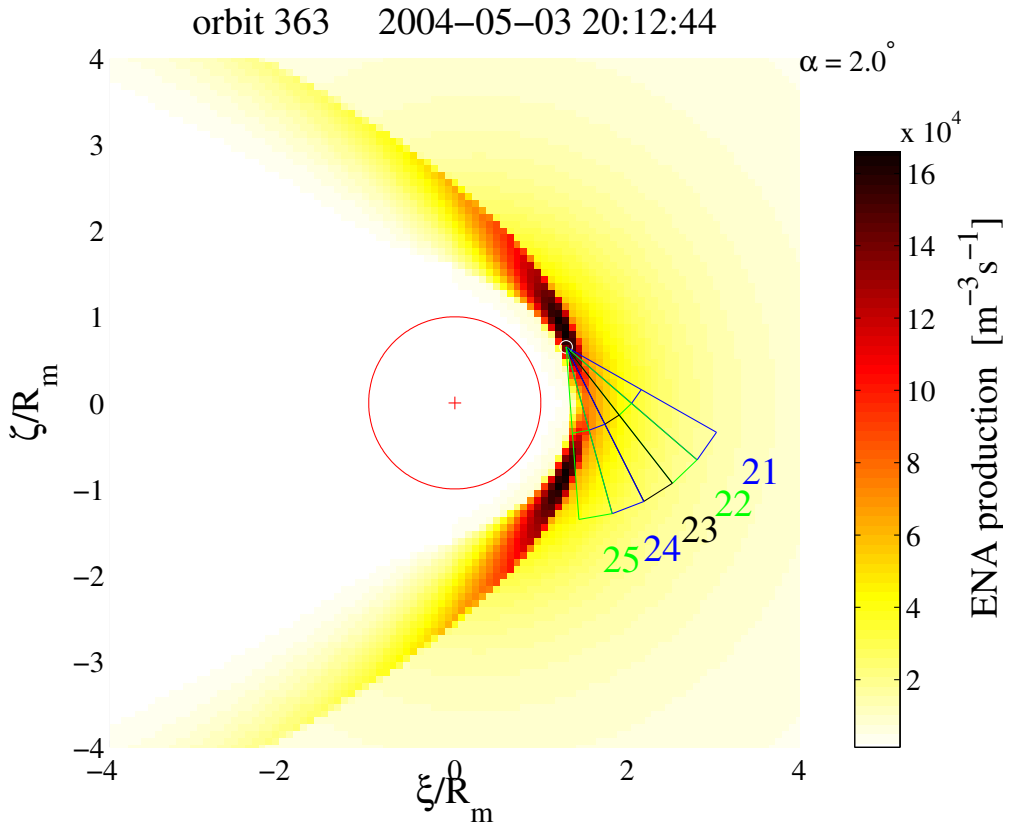

FIG. 4 Spacecraft position and field of view of sectors 21–25 at 20:12:44 UT on 3 May 2004. The colour map shows a simulation of the ENA production rate in a plane that intersects the centre of all NPI sectors. The ξ-axis is the projection of the Mars-Sun line in the NPI plane, and the ζ-axis is perpendicular to both the ξ-axis and the Mars-Sun line.

Simulations 1

ENA simulations:

We have used an empirical model for the plasma flow around Mars based on measurements made with the ASPERA (Automatic Space Plasma Experiment with a Rotating Analyzer) instrument on board the Phobos 2 spacecraft was developed by *Kallio* [2]. This plasma model is combined with a model of the neutral exosphere and models for the charge exchange cross sections.

The number density n_i of neutral species i is modelled as

$$n_i = N_i \exp\left(-\beta_i \left(1/r_0 - 1/r\right)\right) \zeta(\beta_i/r)$$

where r is the distance to the centre of Mars, r_0 is the radius of the exobase, ζ is Chamberlain's partition function [5], and β_i is a constant that is determined by the mass and temperature of each species.

$$\beta_i = GMm_i/(k_B T_i)$$

where G is the gravitational constant, $M = 6.46 \cdot 10^{23}$ kg is the mass of Mars, m_i is the atomic mass of neutral species i, and T_i is the temperature of species i at the exobase. The exobase altitude is assumed to be 170 km.

The simulated ENA flux into the instrument is then

$$w(\theta, \varphi) = \int_0^\infty \int_0^\infty g(\vec{r} + s\vec{d}, -\vec{d}) ds dE$$

where $\vec{r} + s\vec{d}$ is the source point, $-\vec{d}$ the emission direction, and E the emission energy. The differential flux of ENAs with energy E emitted from position $\vec{R}$ in the direction $\vec{D}$ is

$$g(\vec{R}, \vec{D}) = \frac{v}{m} f_{\mathrm{ENA}}(\vec{v}, \vec{R})$$

where

$$f_{\mathrm{ENA}}(\vec{v}, \vec{R}) = \left(n_p(\vec{R}) u(\vec{R}) \sum_i n_i(\vec{R}) \sigma_i \left(u(\vec{R}) \right) \right) \left(\frac{m}{2\pi k_B T_p} \right)^{3/2} e^{-\frac{m}{2k_B T_p} |\vec{v} - \vec{u}|^2}$$

TABLE II Model parameters used by *Holmström et al.* [4] compared to the parameters used here. The exobase is located at 170 km altitude.

Parameter	Holmström	This work
Solar wind		
Plasma density	$2.5 \cdot 10^6 \mathrm{m}^{-3}$	$2.5 \cdot 10^6 \mathrm{m}^{-3}$
Temperature	10 eV	10 eV
Solar wind speed	400 km/s	400 km/s
Geometry		
Bow shock position	$1.55 R_m$	$1.55 R_m$
IMB position	$1.2 R_m$	$1.35 R_m$
IMB penetration	1/6	1/6
Neutral exobase		
H density	9.9×10^{11} m^{-3}	1.98×10^{12} m^{-3}
H temperature	192 K	384 K
H_2 density	$3.8 \cdot 10^{12}$ m^{-3}	7.6×10^{12} m^{-3}
H_2 temperature	192 K	384 K
O_{hot} density	$5.5 \cdot 10^9$ m^{-3}	$1.1 \cdot 10^{10}$ m^{-3}
O_{hot} temperature	$4.4 \cdot 10^3$ K	$8.8 \cdot 10^3$ K
$O_{thermal}$ density	$1.4 \cdot 10^{14}$ m^{-3}	$2.8 \cdot 10^{14}$ m^{-3}
$O_{thermal}$ temperature	173 K	346 K

Comparison

The main peak in the data between 20:11 UT and 20:17 UT can be explained by our ENA production model.

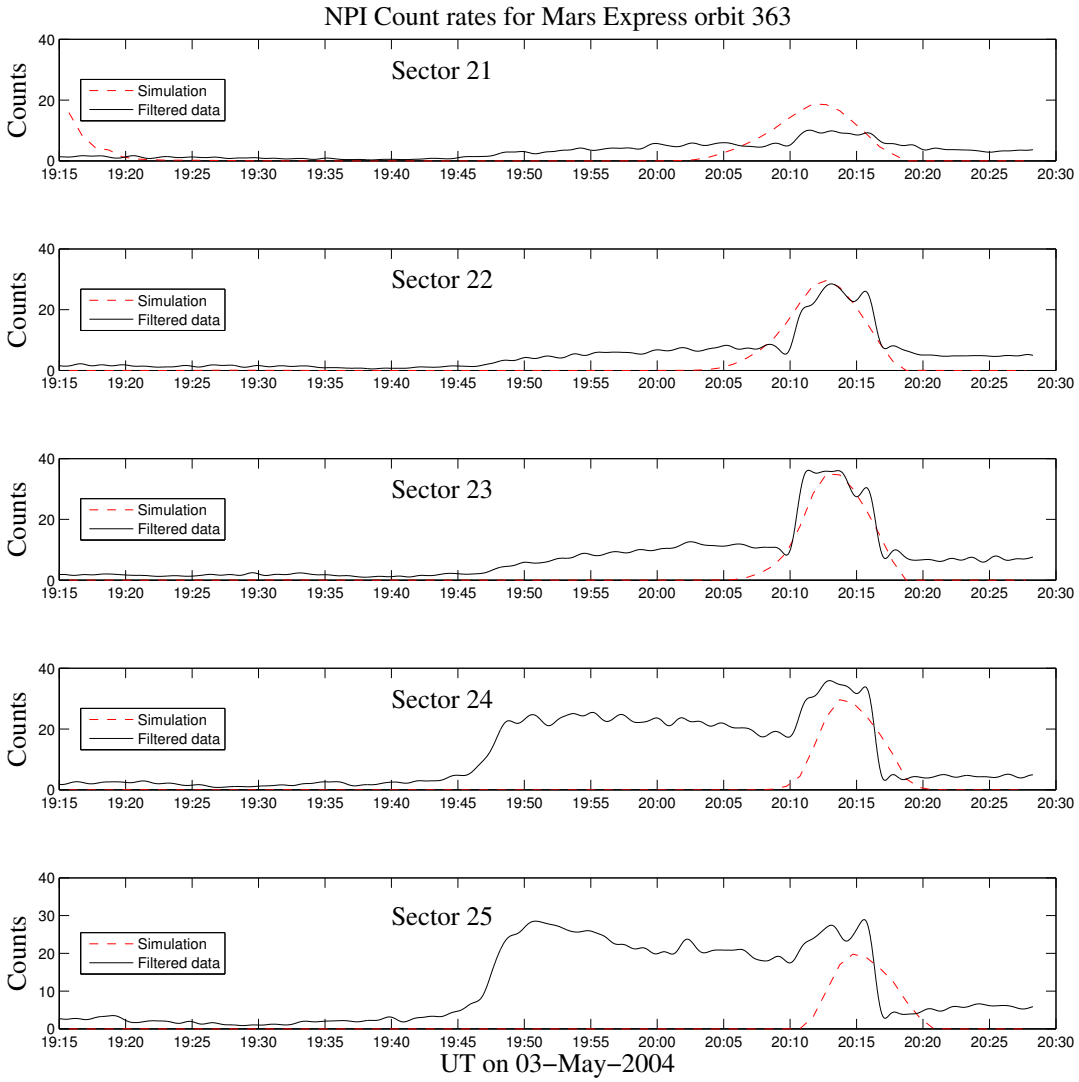

FIG. 5 Simulations and filtered data from MEX orbit 363 and the ASPERA-3 NPI sensor. The highest count rates in sector 23 and 24 correspond to fluxes of $9.9 \times 10^{10}\mathrm{m}^{-2}\mathrm{sr}^{-1}\mathrm{s}^{-1}$ and $9.5 \times 10^{10}\mathrm{m}^{-2}\mathrm{sr}^{-1}\mathrm{s}^{-1}$ respectively.

TABLE III ENA flux observed by the ASPERA-3 NPI and the dark count and sensitivity that was used to calculate the flux.

Sector	Flux $(\mathrm{m}^{-2}\mathrm{sr}^{-1}\mathrm{s}^{-1})$	Dark count	Sensitivity $(\mathrm{m}^{-2}\mathrm{sr}^{-1})$
21	0	11.6	5.2×10^{-10}
22	6.3×10^{10}	11.5	6.8×10^{-10}
23	9.9×10^{10}	9.5	7.9×10^{-10}
24	9.5×10^{10}	10.2	8.0×10^{-10}
25	6.5×10^{10}	11.5	7.9×10^{-10}

Yet unanswered questions

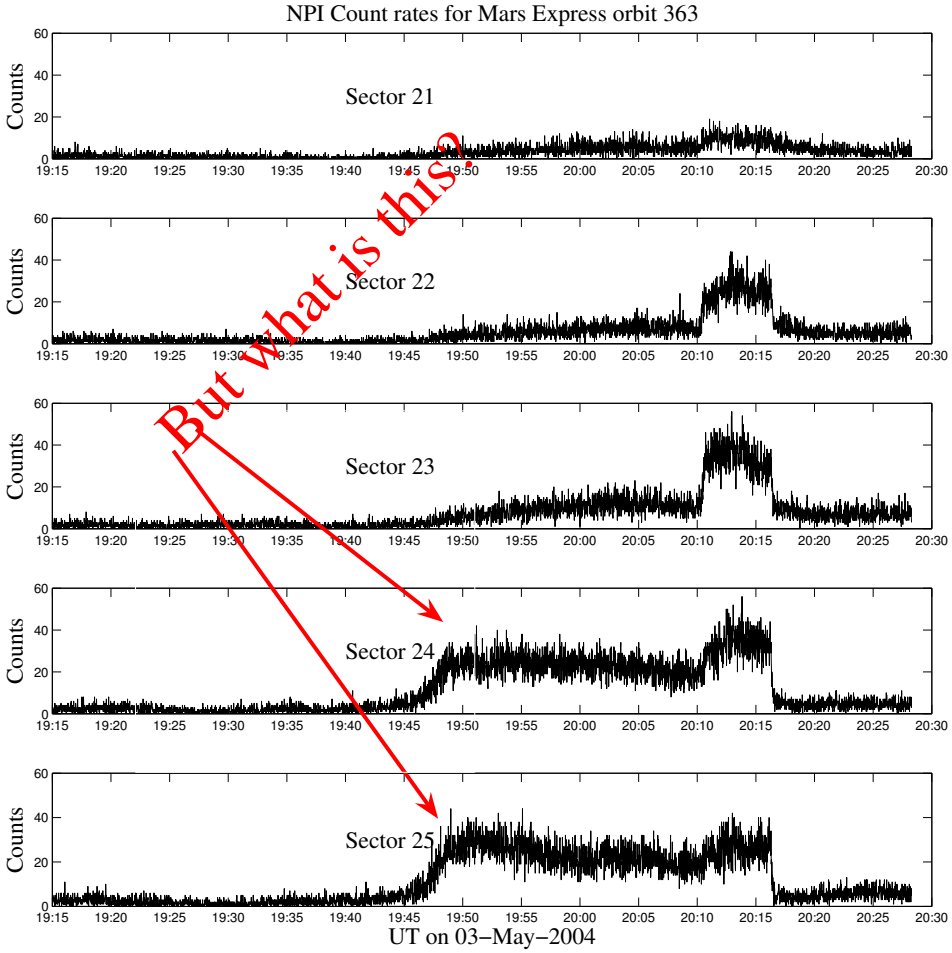

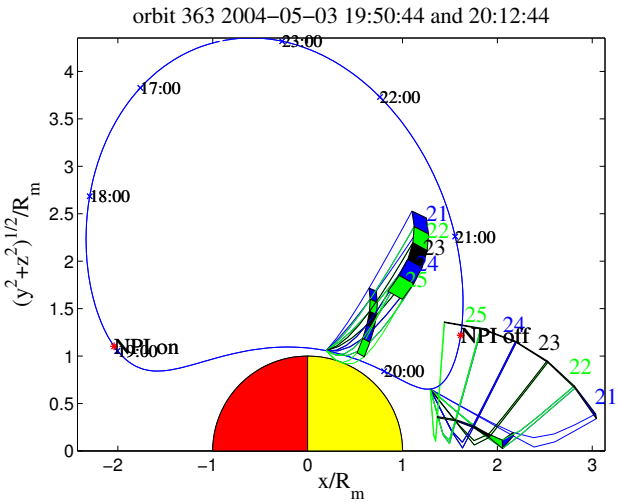

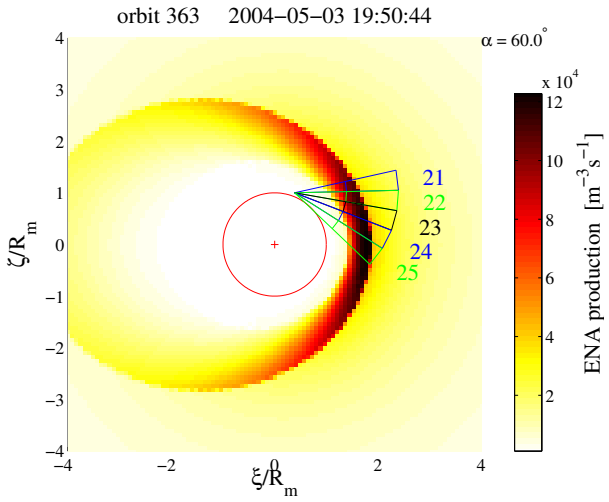

FIG. 6 Spacecraft position and field of view of sectors.

Simulations 2

UV simulations:

We have made a simplified simulation of ultraviolet light from Lyman alpha airglow to investigate the possible contamination of the data by UV photons. The count rate caused by UV photons is estimated by a line of sight integral over the density of neutral hydrogen in the exosphere

$$R_{UV} = A\sigma_{abs}Q\phi_s\frac{\Omega}{4\pi}\int_{LOS} n_H ds$$

where $A = 5.25 \times 10^{-5}\mathrm{m}^2$ is the detector area, $\sigma_{abs} = 1.8 \times 10^{-24}\mathrm{m}^2$ the photo absorption cross section, $\phi = 3.99 \times 10^{15}\mathrm{m}^{-2}\mathrm{s}^{-1}$ the solar Lyman alpha flux, $Q = 5 \times 10^{-6}$ the quantum efficiency of the NPI, Ω the solid angle of the field of view, and n_H is the density of neutral hydrogen in the exosphere. The value for the solar Lyman alpha is obtained from the Solar200 model [6]. Analogously to the ENA simulations described above a weighted average is then formed using the measured relative sensitivities for different angles of incidence. The quantum efficiency and the relative directional sensitivities were obtained in measurements on a copy of the flight instrument. This introduces an uncertainty of the absolute count rate, but the simulation result can still serve as a relative measure of the contribution from ultraviolet light, and the shape of the curves shown below can be compared to the shape of the curves showing observed count rate on page 3.

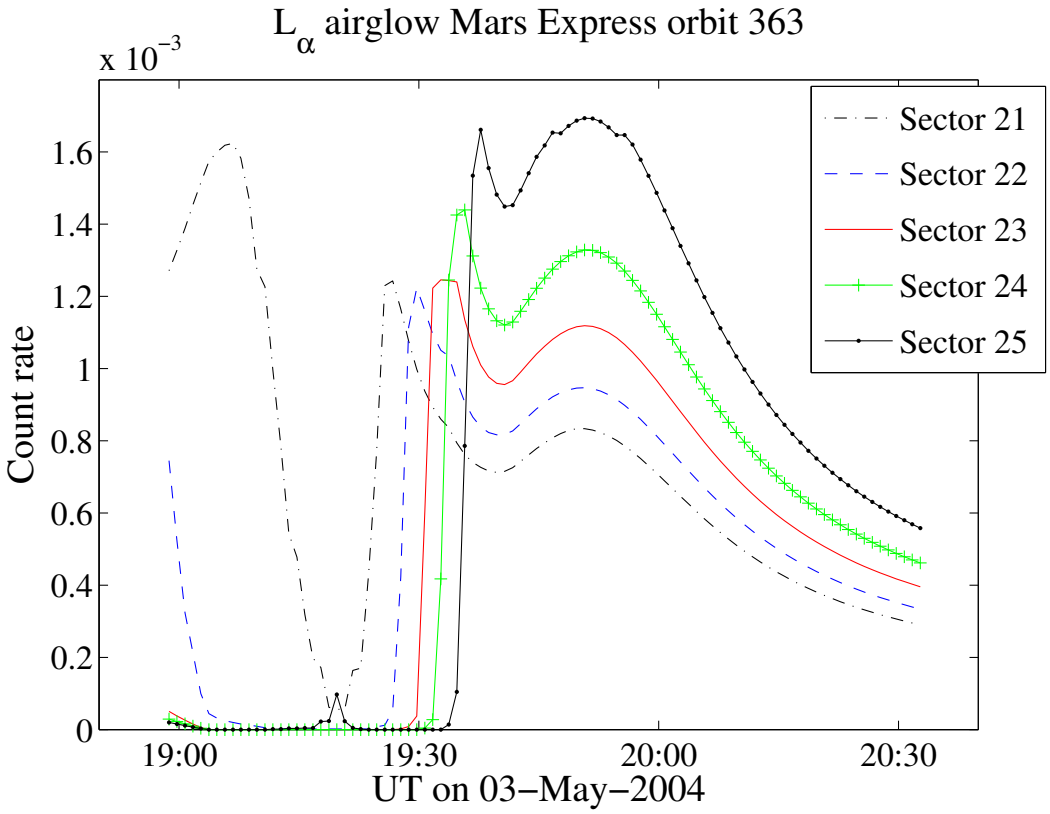

FIG. 7 A simulation of the count rate caused by Lyman alpha airglow from the Martian hydrogen corona.

Summary and Conclusions

- We have presented data from the Neutral particle imager of the ASPERA-3 instrument on ESA's Mars Express mission. During orbit 363 between 20:11 and 20:17 UT on 3 May 2004 a peak appeared in the observed count rate.
- The maximum flux is approximately 10^{11} $\mathrm{m^{-2}sr^{-1}s^{-1}}$ in agreement with the predictions by *Holmström et al.* [4].
- The data agrees with simulations using an IMB position, defined as the planetocentric distance to the IMB along the Mars-sun line, of $1.35R_m$, and an, analogously defined, bow shock position of $1.55R_m$.
- The exosphere parameters were varied to achieve better agreement for the value of the count rate at the main peak. The set of parameters arrived at in this way is not a unique solution. There are other possible ways to vary the parameters to obtain an equally good agreement. One application of ENA measurements is parameter extraction [7]. Future work may improve our abilities to extract parameters from these ENA measurements.
- The peak at 19:50 and the following slowly decreasing plateau seen in some of the sections is not yet understood.
- This study shows that the general picture of the generation of ENAs at Mars is correct. ENAs are generated in the between the bow shock and the induced magnetosphere boundary, and the flux agrees with predicted values. Now that a general agreement has been confirmed ENA measurements can be used in future work for automated parameter extraction; to study mass loading, the shape and variability of plasma boundaries; and for comparison between different Mars-solar wind interaction models.

---

* Electronic address: herbert.gunell@physics.org; URL: http://www.irf.se/~herbert
† Currently at NASA Goddard Space Flight Center, Laboratory for Solar and Space Physics, Mail Code 612.2, Greenbelt, MD 20771, USA

[1] Barabash, S., R. Lundin, H. Andersson, et al., ASPERA-3: Analyser of space plasmas and energetic ions for Mars express, *ESA Special Publication*, pp. 121–139, SP-1240, 2004.
[2] Kallio, E., An empirical model of the solar wind flow around Mars, *J. Geophys. Res.*, *101*, 11,133–11,147, 1996.
[3] Kallio, E., J. G. Luhmann, and S. Barabash, Charge exchange near Mars: The solar wind absorption and energetic neutral atom production, *J. Geophys. Res.*, *102*, 22,183–22,197, 1997.
[4] Holmström, M., S. Barabash, and E. Kallio, Energetic neutral atoms at Mars I: Imaging of solar wind protons, *J. Geophys. Res.*, *107*(A10), 1277, doi:10.1029/2001JA000325, 2002.
[5] Chamberlain, J. W., and D. M. Hunten, *Theory of planetary atmospheres*, second ed., Academic Press, inc., San Diego, California, 1987.
[6] Tobiska, W. K., T. Woods, F. Eparvier, R. Viereck, L. Floyd, D. Bouwer, G. Rottman, and O. R. White, The SOLAR2000 empirical solar irradiance model and forecast tool, *Journal of Atmospheric and Terrestrial Physics*, *62*, 1233–1250, 2000.
[7] Holmström, M., and E. Kallio, The solar wind interaction with Venus and Mars: Energetic neutral atom and X-ray imaging, *Adv. Space Res.*, *33*(2), 187–193, 2004.